ELSEVIER

Thermochimica Acta 284 (1996) 213–227

thermochimica acta

Preparation and thermal decomposition of various forms of strontium oxalate[1]

E. Knaepen, J. Mullens *, J. Yperman, L.C. Van Poucke

Laboratory of Inorganic and Physical Chemistry, Limburgs Universitair Centrum, B-3590 Diepenbeek, Belgium

Abstract

Strontium oxalate exists in two different forms: the neutral strontium oxalate hydrate, $SrC_2O_4 \cdot xH_2O$, and the acid salt of strontium oxalate, $SrC_2O_4 \cdot yH_2C_2O_4 \cdot xH_2O$. Depending on the concentration of oxalic acid and ammonium oxalate as precipitating agents, both forms can be obtained. At a sufficiently low pH, the stoichiometric compound $SrC_2O_4 \cdot 1/2H_2C_2O_4 \cdot H_2O$ is formed. The thermal decomposition of the different strontium oxalates is studied in different atmospheres using DSC, and TGA coupled with FTIR and MS. The TGA–EGA spectra indicate that the anhydrous acid oxalate decomposes with the release of H_2O, CO, CO_2 and formic acid.

Keywords: Strontium oxalate; Thermal decomposition; DSC; TGA; FTIR; MS

1. Introduction

The preparation of strontium oxalate is part of the study of oxalate precursors for the synthesis of BiSCCO superconductors. These superconductive ceramic materials are usually prepared by the solid state reaction which consists of a thermochemical reaction of Bi_2O_3, $SrCO_3$,$CaCO_3$ and CuO. This mixed-oxide/carbonate synthesis, however, has several disadvantages: microscopic compositional inhomogeneities [1] resulting in long calcination and sintering times, nonuniformity of particle size and

* Corresponding author.

[1] Presented at the 24th North American Thermal Analysis Society Conference, San Francisco, CA, U.S.A., 10–13 September 1995

PII S0040-6031(96)02863-8

shape, and lack of reproducibility. In order to improve the homogeneity of the superconductive materials, various alternative methods have received special attention and interest during recent years.

Among the chemical routes, sol-gel [2], dry-spraying [3], and coprecipitation techniques [4–7] are most widely investigated for ceramic powder preparation. These chemical methods have indeed important advantages, such as the production of more homogeneous powders, good stoichiometric control and shorter thermal treatment [8]. Among the precipitation-filtration techniques [4], the most used precipitating agent is the oxalate ion [5–6]. Oxalates form solid solutions and can easily be decomposed [7].

The decomposition of oxalates can be studied by thermal analysis of the different components. The thermal decomposition of various forms of barium oxalate has been extensively discussed by Walter-Levy and Laniepce [9], Mutin and Watelle-Marion [10] and Bhatti and Dollimore [11]. Barium oxalate has been reported to exist in two distinct forms; the neutral barium oxalate with various hydrated forms, and the acid salt of barium oxalate.

In this paper we report the preparation and thermal analysis of various forms of strontium oxalate, comparable with the two distinct forms of barium oxalate. The obtained solids were identified by X-ray diffraction (XRD) and characterized by particle size distribution measurements and scanning electron microscope (SEM). The thermal behavior of the oxalate powders was investigated in inert oxidizing atmospheres employing thermogravimetric analysis (TGA) and differential scanning calorimetry (DSC). To identify the evolved gases, TGA experiments were coupled with fourier transform infrared spectroscopy (FTIR) and mass spectrometry (MS).

2. Experimental

2.1. Methods and apparatus

The determination of Sr^{2+} in the precipitates was performed by Atomic Emission Spectrometry (AES) using a Perkin-Elmer 703 Atomic Absorption Spectrometer. The emission was measured at 460.7 nm with the use of the high-temperature N_2O–acetylene flame. In order to suppress the ionization processes in this flame, KCl was added to the analysed solutions. Soultions of known concentrations (0.5, 1,2 ppm) for the construction of the calibration graphs had the same concentration of KCl as used in the sample solutions.

The thermogravimetric measurements were performed with a TA Instruments Model 951–2000 (temperature range, ambient to 1200°C). The evolved gases were examined by a Fisons-VG Thermolab MS and a Bruker FTIR IFS 48, both coupled with a TGA unit. The FTIR has a resolution of 8 cm^{-1}. DSC analysis was carried out by heating the obtained solids in a DSC 910–2000 analyser at 10°C min^{-1} from room temperature up to 600°C. A Siemens D-5000 diffractometer using a Cu K_α line was used to record the XRD spectra. The measurements were performed at room temperature in

air under normal pressure. The crystal sizes and shapes were examined in a Philips 535M SEM. The surface of the samples was coated with a thin, uniform, electrically conductive gold film. The excitation voltage used was 6 kV. The particle size distribution was measured with a Malvern Mastersizer / E.

2.2. Materials

The following starting products were used: $Sr(NO_3)_2$ (Merck p.a.), $H_2C_2O_4 \cdot 2H_2O$ (Merck p.a.) and $(NH_4)_2C_2O_4 \cdot H_2O$ (Merck p.a.). All three compounds are fine, white powders. The amount of hydration water was checked by TGA. A weight change during the dehydration step of 28.7% and 12.7% respectively for oxalic acid and ammonium oxalate confirmed that each mole of compound contains respectively one and two moles of water.

2.3. Preparation of strontium oxalate

Strontium oxalate was made by adding an aqueous solution of $Sr(NO_3)_2$ to an aqueous solution of $H_2C_2O_4$ and $(NH_4)_2C_2O_4$. The concentration of Sr^{2+} was fixed at 0.2 M. A series of samples was prepared using different concentration ratios of ammonium oxalate and oxalic acid. The white precipitates were prepared in a thermostated cage (25.0 ± 0.2°C) by mixing the oxalate solution with the strontium nitrate solution by two motor-driven burettes (Schott Geräte T100) at the same speed and under continuous stirring. The obtained coprecipitates were filtered through a 0.45 micron Millipore filter and washed with bidistilled water. Finally, the powders were dried in air.

3. Results

3.1. Determination of Sr^{2+}

The amount of precipitated SrC_2O_4 was determined indirectly by analysis of the supernatants for residual Sr^{2+} cations after precipitating oxalate as strontium oxalate. The results are listed in Table 1. The amount Sr^{2+} in terms of mol l^{-1} refers to the amount (mol) of precipitate formed by mixing 500 ml of both starting solutions. The composition of the samples, prepared in different concentrations of $H_2C_2O_4$ and $(NH_4)_2C_2O_4$, is given in Table 2. Comparable results have been reported [12] for barium oxalate which is also formed as pure BaC_2O_4 in an excess of $(NH_2)_4C_2O_4$. From equal amounts of $H_2C_2O_4$ and $(NH_4)_2C_2O_4$, the acid form $BaC_2O_4 \cdot xH_2C_2O_4$ was synthesized with x ranging from 0.1 to 0.93.

3.2. XRD analysis

XRD measurements were performed to identify the prepared solids. Samples 1 and 2 were identified as single phases, corresponding to $SrC_2O_4 \cdot H_2O$ [13]. From X-ray

Table 1
Results of Sr^{2+} determination for 9 different samples

Sample	Start solution 1/mol l^{-1}		Start solution 2/mol l^{-1}	Amount/mol l^{-1}
	$[Sr(NO_3)_2]$	$[H_2C_2O_4]$	$[(NH_4)_2C_2O_4]$	
1	0.2	0.1	0.3	0.09962
2	0.2	0.2	0.2	0.09241
3	0.2	0.3	0.1	0.07581
4	0.2	0.4		0.06715
5	0.2	0.5	–	0.07635
6	0.2	0.6	–	0.08346
7	0.2	0.7	–	0.08978
8	0.2	0.8		0.09046
9	0.2	0.9		0.09252

Table 2
% mass loss and composition for each compound

Sample	dehydration	Decomposition of $H_2C_2O_4$	SrC_2O_4 ↓ $SrCO_3$	$SrCO_3$ ↓ SrO	Total mass loss		Composition
					exp.	theor.	
1	9.5	–	14.1	22.7	46.3	46.5	$SrC_2O_4 \cdot H_2O$
2	9.5	–	13.8	23.1	46.4	46.5	$SrC_2O_4 \cdot H_2O$
3	11.3	–	13.5	22.7	47.5	47.5	$SrC_2O_4 \cdot 1.25H_2O$
4	14.3	3.8	12.8	20.5	51.4	51.7	$SrC_2O_4 \cdot 0.09H_2C_2O_4 \cdot 1.7H_2O$
5	8.8	16.6	11.4	19.0	55.8	56.0	$SrC_2O_4 \cdot 0.43H_2C_2O_4 \cdot 1.2H_2O$
6	7.9	18.5	11.4	18.8	56.6	56.6	$SrC_2O_4 \cdot 1/2H_2C_2O_4 \cdot H_2O$
7	7.9	18.6	11.4	18.5	56.4	56.6	$SrC_2O_4 \cdot 1/2H_2C_2O_4 \cdot H_2O$
8	7.8	18.5	11.3	18.9	56.5	56.6	$SrC_2O_4 \cdot 1/2H_2C_2O_4 \cdot H_2O$
9	7.7	18.6	11.4	18.7	56.4	56.6	$SrC_2O_4 \cdot 1/2H_2C_2O_4 \cdot H_2O$

analysis of samples 3, 4 and 5, one can conclude that these solids are composed of several phases. In Fig. 1a, all the significant peaks in the XRD spectrum of sample 4 in the 2θ range from 10° to 50° are identified by comparing the d-values of the experimental spectrum with those extracted from the JCPDS-ICDD file [13, 14]. Samples 6–9 are again single phases, identified as $SrC_2O_4 \cdot 1/2H_2C_2O_4 \cdot H_2O$. The XRD spectrum of sample 9 is given in Fig. 1b and confirms that $SrC_2O_4 \cdot 1/2H_2C_2O_4 \cdot H_2O$ is obtained by adding 0.2 M $Sr(NO_3)_2$ to an aqueous solution of 0.9 $MH_2C_2O_4$.

3.3. Particle size distribution and SEM

The volume size distribution curve of $SrC_2O_4 \cdot H_2O$ particles shows a small maximum at 0.5 μm and a distribution between 10 and 35 μm, with a second, higher maximum at 22.5 μm. In these measurements the particles are assumed to be spherical.

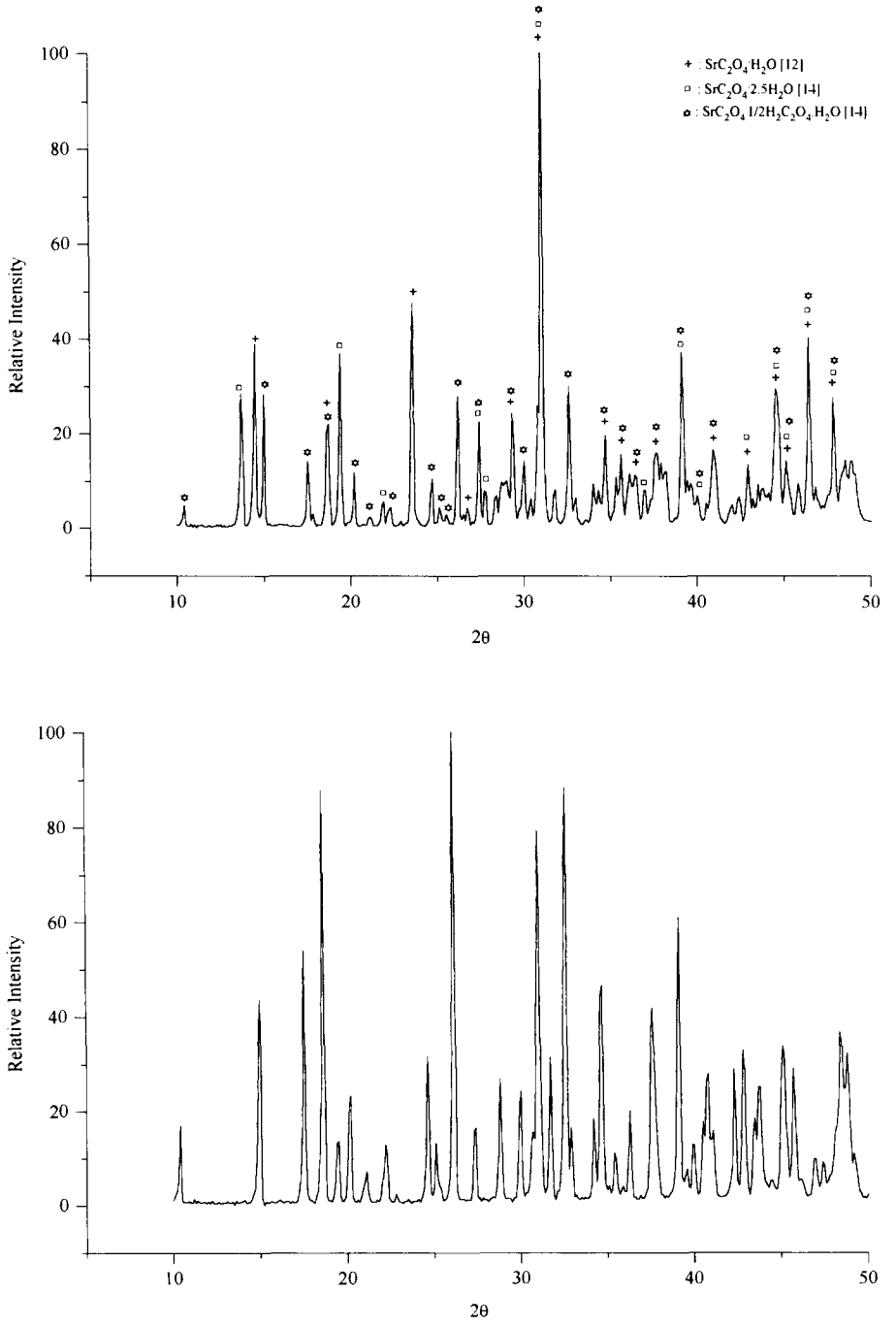

Fig. 1. XRD spectra of: a, sample 4 ($SrC_2O_4 \cdot 0.09H_2C_2O_4 \cdot 1.7H_2O$); b, sample 9 ($SrC_2O_4 \cdot \frac{1}{2} H_2C_2O_4 \cdot H_2O$).

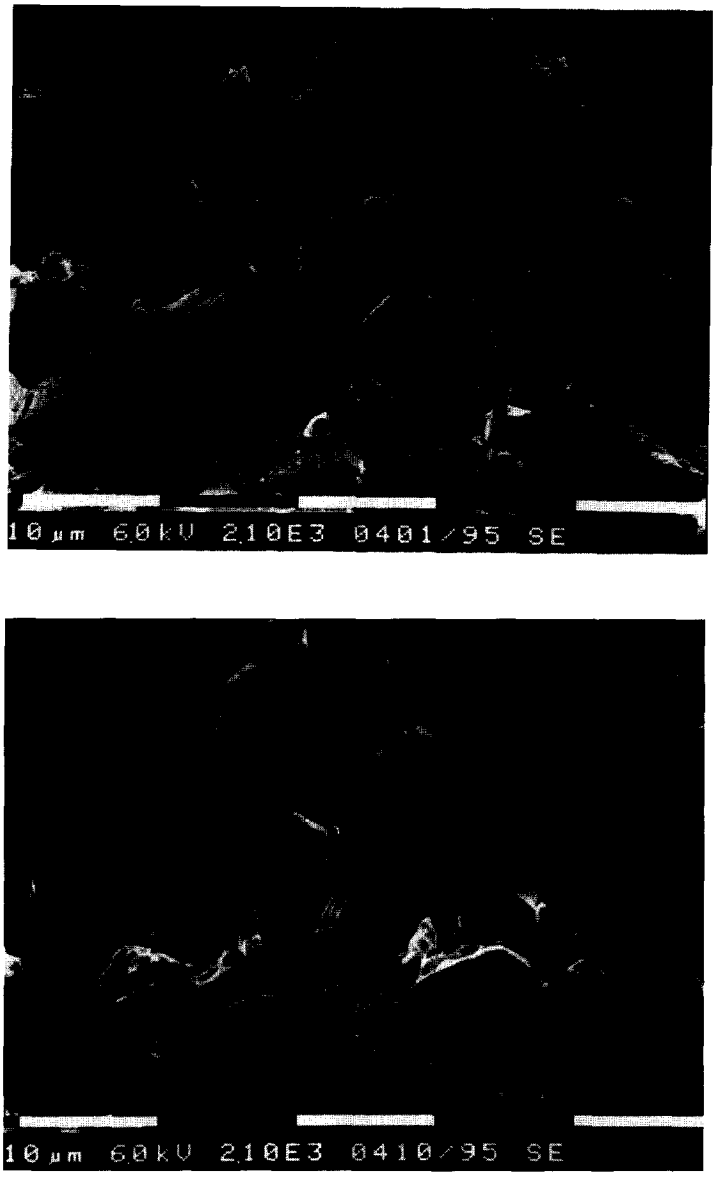

Fig. 2. SEM of: a, sample 1 ($SrC_2O_4 \cdot H_2O$); b, sample 7($SrC_2O_4 \cdot \frac{1}{2}H_2C_2O_4 \cdot H_2O$). Scale bat, 10$\mu$m.

The real morphology, however, is shown in the SEM micrograph of Fig. 2a. This picture confirms the results obtained from particle size measurements. The particles of $SrC_2O_4 \cdot 1/2H_2C_2O_4 \cdot H_2O$ are bigger, with a distribution between 15 and 60 μm and a maximum at 35.5 μm. Fig. 2b shows the corresponding SEM picture.

3.4. Thermal analysis

The thermal behavior of $SrC_2O_4 \cdot yH_2C_2O_4 \cdot xH_2O$ (samples 1, 4, 5 and 6) is shown in Fig. 3 and Table 2. Table 2 lists the percentage mass loss in Ar for each decomposition step of each compound and the composition that fits with this mass loss. It is shown that varying the concentration of oxalic acid and ammonium oxalate (samples 1–9) produces forms of strontium oxalate with different composition. At sufficiently low pH (starting from sample 4), the acid form of SrC_2O_4 is formed, moving to a constant composition for samples 6–9. Table 2 shows a good agreement between the theoretical and experimental total mass loss during a TGA experiment as well for the neutral and acid forms of strontium oxalate. The TGA experiments are illustrated in Fig. 3. These results, together with the identification of the evolved gases by MS (Figs. 4 and 5) and FTIR (Fig. 6 and Table 3), are related to the subsequent decomposition steps obtained by TGA, see discussion below. The inert working condition of the TA equipment in Ar was checked regularly by the copper oxalate test as described elsewhere [15]. This test ensures that all TA measurements are performed in a completely oxygen-free atmosphere. Table 3 summarizes the TGA–FTIR results for the neutral and acid oxalate.

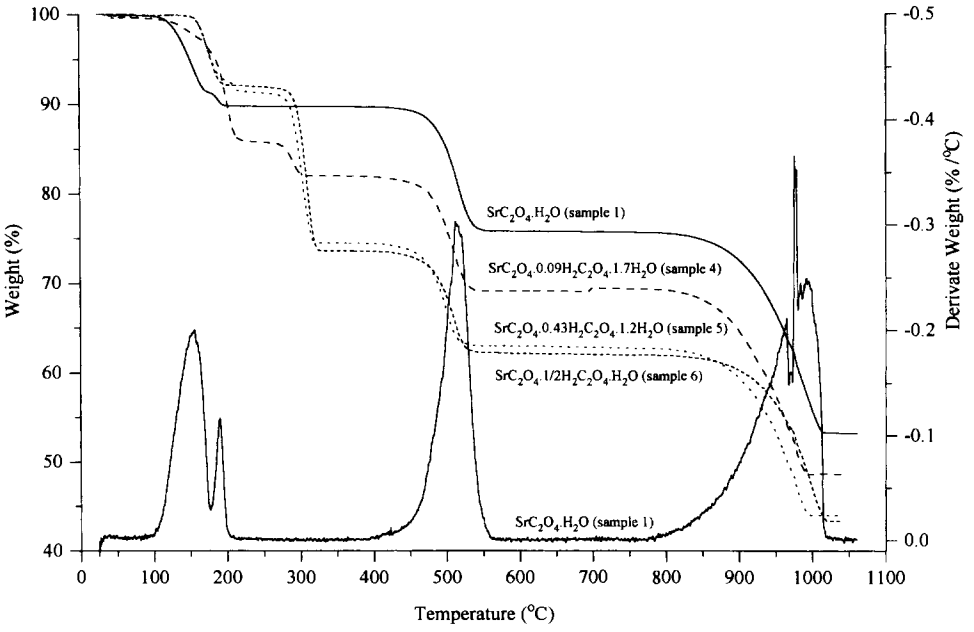

Fig. 3. TGA of $SrC_2O_4 \cdot H_2O$ (sample 1) and $SrC_2O_4 \cdot yH_2C_2O_4 \cdot xH_2O$ (samples 4, 5 and 6) in Ar; heating rate, 10°C min^{-1}.

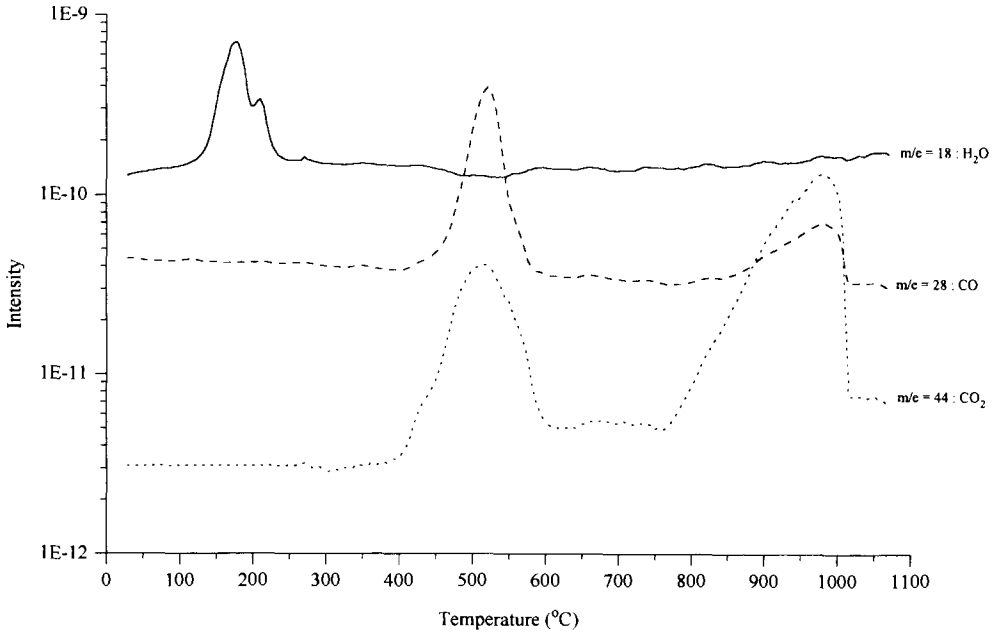

Fig. 4. Mass spectrum of gases released by the decomposition of $SrC_2O_4 \cdot H_2O$ (sample 1) in Ar.

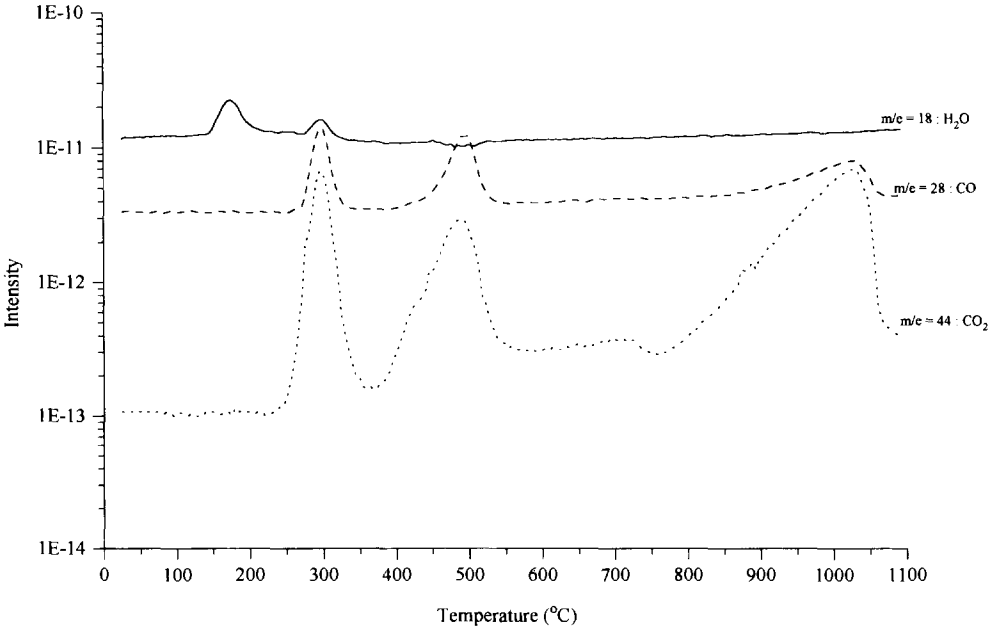

Fig. 5. Mass spectrum of gases released by heating $SrC_2O_4 \cdot 1/2H_2C_2O_4 \cdot H_2O$ (sample 6) in Ar.

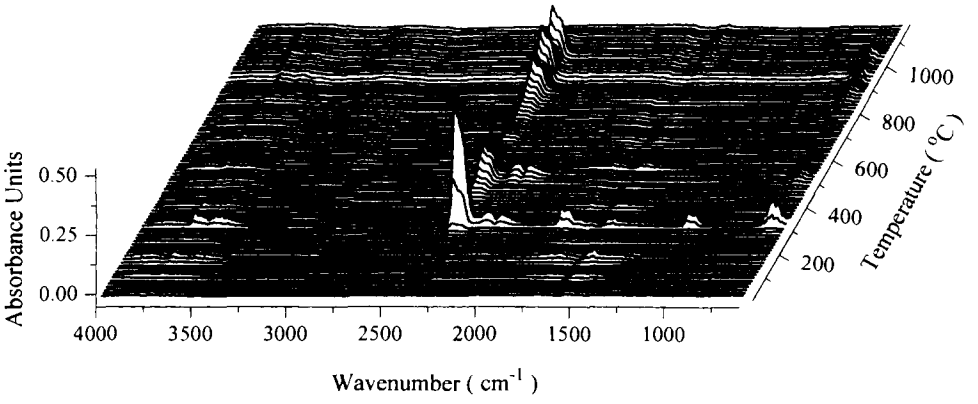

Fig. 6. FTIR stack plot of gases released by heating $SrC_2O_4 \cdot 1/2H_2C_2O_4 \cdot H_2O$ (sample 6) in Ar.

Table 3
Vibrational wavenumber and band assignments in the FTIR spectrum of the gases released by heating $SrC_2O_4 \cdot H_2O$ (1) and $SrC_2O_4 \cdot \frac{1}{2}H_2C_2O_4 \cdot H_2O$ (6)

Decomposition step	Sample	$\bar{\nu}$ (wavenumber)/cm^{-1}	Band assignments
Dehydration	1 + 6	3900–3500	ν_{as}(HOH) + ν_s(HOH)
		2000–1250	δ(HOH)
Decomposition of $H_2C_2O_4$	6	3733–3591	ν_{as}(HOH) + ν_s(HOH)
		2360–2328	ν_{as}(OCO)
		2182–2114	ν(CO)
		1793–1750	ν(C=O)
		1600–1509	δ(HOH)
		1121–1080	ν(C–O)
		671–649	δ(OCO)
$SrC_2O_4 \rightarrow SrCO_3$	1 + 6	2353–2329	ν_{as}(OCO)
		2178–2115	ν(OCO)
		670–649	δ(OCO)
$SrCO_3 \rightarrow SrO$	1 + 6	2358–2329	ν_{as}(OCO)
		670–650	δ(OCO)

4. Discussion and conclusion

4.1. Decomposition of the neutral oxalate $SrC_2O_4 \cdot H_2O$ in Ar (sample 1)

4.1.1. Formation of the carbonate

The following reactions describe the decomposition of the oxalate to the carbonate. The temperatures given in the following scheme are taken from the MS results (Fig. 4) because this technique is extremely sensitive and allows the detection of the first traces

before this can be seen in TGA and DTG.

$$SrC_2O_4 \cdot H_2O \xrightarrow[\text{endo}]{130\text{–}250^\circ C} SrC_2O_4 + H_2O \quad [\Delta m(1)\text{: theor. 9.3\%; exp. 9.5\%}] \ (1)^*$$

$$SrC_2O_4 \xrightarrow[\text{endo}]{420\text{–}590^\circ C} SrCO_3 + CO \quad [\Delta m(2)\text{: theor. 14.5\%; exp. 14.1\%}] \qquad (2a)^*$$

$$2CO \underset{\text{endo}}{\overset{\text{exo}}{\rightleftharpoons}} CO_2 + C \qquad (2b)$$

For reaction (1), the mass spectrometer results (Fig. 4) indicate that the primary fragment for the first mass loss corresponds with $m/e = 18$, thereby confirming that the low temperature mass loss is attributed to the loss of coordinated water. From FTIR results (Table 3), it is also shown that water is the only gas evolved. DSC analysis (Fig. 7) shows an endothermic peak with two minima at 169 and 190°C, indicating that the dehydration takes place in two steps. These results are confirmed by the deriviate curve of the TGA plot of sample 1 (Fig. 3).

For reaction (2a), the percentage mass loss between 420 and 590°C correponds to the formation of strontium carbonate from anhydrous strontium oxalate by the evolution of CO. The mass spectrometer, however, detected CO_2 ($m/e = 44$) concurrent with CO evolution ($m/e = 28$) in an inert atmosphere. The FTIR spectrum (Table 3) corresponding with this temperature interval also shows peaks due to both CO and CO_2

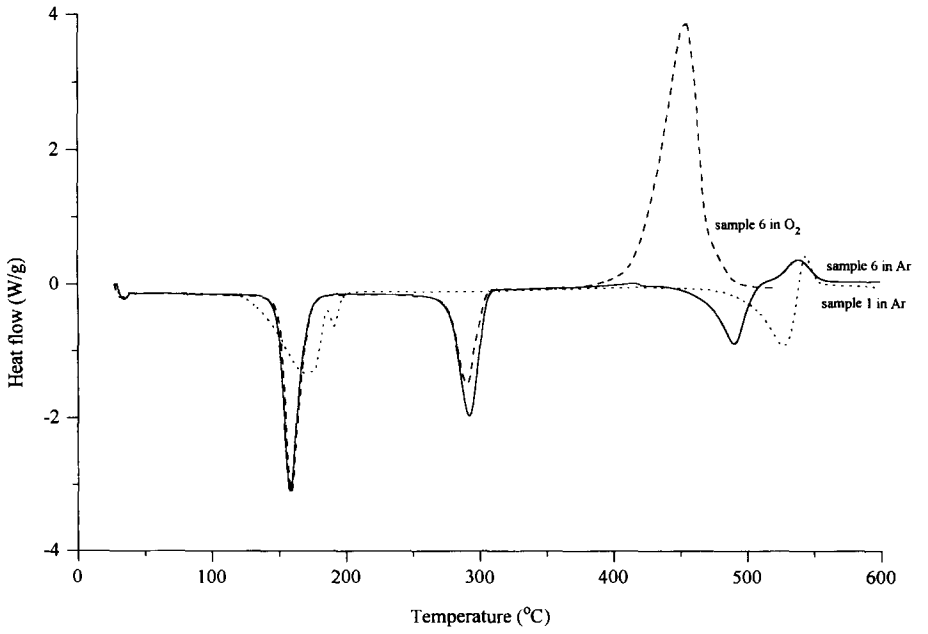

Fig. 7. DSC of $SrC_2O_4 \cdot H_2O$ (sample 1) and $SrC_2O_4 \cdot \frac{1}{2}H_2C_2O_4 \cdot H_2O$ (sample 6) in Ar and in O_2; heating rate, 10°C min^{-1}.

vibrations. Since carbon dioxide is detected during the conversion into the carbonate in an inert atmosphere by both TGA–MS and TGA–FTIR, the evolution of CO_2 is attributed to a disproportionation reaction (2b) of evolved CO to yield CO_2 and carbon [16]. After DSC measurements, traces of black carbon are seen on the cooled residue, confirming that carbon is formed. Fig. 7 shows clearly that endothermic carbonate formation is followed by exothermic disproportionation.

4.1.2. Decomposition of the carbonate

In the temperature domain between 770 and 1020°C, the TGA curve (Fig. 3) show an overall weight loss, due to the decomposition into SrO. The shape of the derivate TGA curve (Fig. 3) suggests a decomposition in two steps; this is in accordance with the results of Dollimore and Griffiths, [17] who studied the decomposition of strontium oxalate by DTA and who reported an endothermic phase change in the carbonate between 911 and 924°C,

$$SrCO_3 \xrightarrow[\text{endo}]{770\ 1020\ C} SrO + CO_2 \quad [\Delta m(3)\text{: theor. } 22.7\%\text{; exp. } 22.7\%] \tag{3}$$

For reaction (3), the last mass loss corresponds with the decomposition of the carbonate to the oxide. The FTIR spectrum (see Table 3) shows only peaks due to CO_2 vibrations. The mass spectrum of the released gases (Fig. 4) shows peaks at $m/e = 44$ and at $m/e = 28$. The presence of the latter peak is consequently assigned to fragmentation of CO_2 in the mass spectrometer.

4.2. Decomposition of the acid salt $SrC_2O_4 \cdot 1/2H_2C_2O_4 \cdot H_2O$ in Ar (sample 6) [18]

The acid salt (sample 6) decomposes in four well-defined steps between 145 and 1060°C. For a complete description of this decomposition process, again TGA coupled with MS and with FTIR and DSC are used (Figs. 5, 6 and 7).

4.2.1. Formation of the carbonate

$$SrC_2O_4 \cdot 1/2H_2C_2O_4 \cdot H_2O \xrightarrow[\text{endo}]{145\text{–}210\ C} SrC_2O_4 \cdot 1/2H_2C_2O_4 + H_2O \tag{4}*$$

$$[\Delta m(4)\text{ theor. } 7.6\%\text{; exp. } 7.9\%]$$

$$SrC_2O_4 \cdot 1/2H_2C_2O_4 \xrightarrow[\text{endo}]{240\text{–}350\ C} SrC_2O_4 + 1/2HCOOH + 1/2CO_2 \tag{5a}*$$

$$SrC_2O_4 \cdot 1/2H_2C_2O_4 \xrightarrow[\text{endo}]{240\text{–}350\ C} SrC_2O_4 + 1/2H_2O + 1/2CO + 1/2CO_2 \tag{5b}$$

$$[\Delta m(5)\text{ theor. } 18.9\%\text{; exp. } 18.5\%]$$

$$SrC_2O_4 \xrightarrow[\text{endo}]{380\ 550\ C} SrCO_3 + CO \quad [\Delta m(6)\text{ theor. } 11.7\%\text{; exp. } 11.4\%] \tag{6a}*$$

$$2CO \underset{\text{endo}}{\overset{\text{exo}}{\rightleftharpoons}} CO_2 + C \tag{6b}$$

For reaction (4), DSC analysis (Fig. 7) shows an endothermic peak with a minimum at 164°C. In the TGA curve a plateau is produced at 7.9% mass loss, which corresponds to dehydration by the loss of one molecule of water. In the temperature domain 145–210°C the FTIR plot in Fig. 6 shows a large peak at 3500–3600 cm^{-1} (antisymmetric and symmetric OH stretching) [19] and one at 1500–1600 cm^{-1} (HOH bending). The spectrum has a large rotation–vibration fine structure.

For reaction (5a), DSC analysis of sample 6 (Fig. 7) shows a large endothermic peak between 260 and 310°C due to the decomposition of oxalic acid from the anhydrous acid oxalate. Dollimore and Griffiths [17] studied the thermal decomposition of oxalic acid by DTA, resulting in an overlapping series of endothermic reactions comprising dehydration, volatization and decomposition. In the present work, the decomposition of oxalic acid was studied by DSC and TGA (Fig. 8a) with the simultaneous analysis of the evolved gases by FTIR (Fig. 8b). This supplementary study on the decomposition of $H_2C_2O_4 \cdot 2H_2O$ was done in order to deduce the decomposition of $H_2C_2O_4$ bound on the oxalate. The first weight loss in Fig. 8a corresponds to the endothermic dehydration of two water molecules ($\Delta m_{exp} = 28.5\%$; $\Delta m_{theor} = 28.6\%$). After dehydration, $H_2C_2O_4$ is completely decomposed. In Fig. 8b, the FTIR spectrum of the evolved gases during decomposition of dehydrated oxalic acid is compared with that during the sublimation of formic acid. From this comparison, it is deduced that $H_2C_2O_4$ decomposes with the release of CO_2 ($\bar{\nu} = 2357–2321\ cm^{-1}$ and $669–640\ cm^{-1}$), H_2O ($\bar{\nu} = 3730–3548\ cm^{-1}$) and gaseous formic acid ($\bar{\nu} = 2959–2321\ cm^{-1}$ (ν_{CH}), $1793–1750\ cm^{-1}$ ($\nu_{C=O}$) and $1121–1080\ cm^{-1}$ ($\nu_{C\ O}$)) at about 200°C. Table 3 shows that all these peaks (except ν_{CH} due to

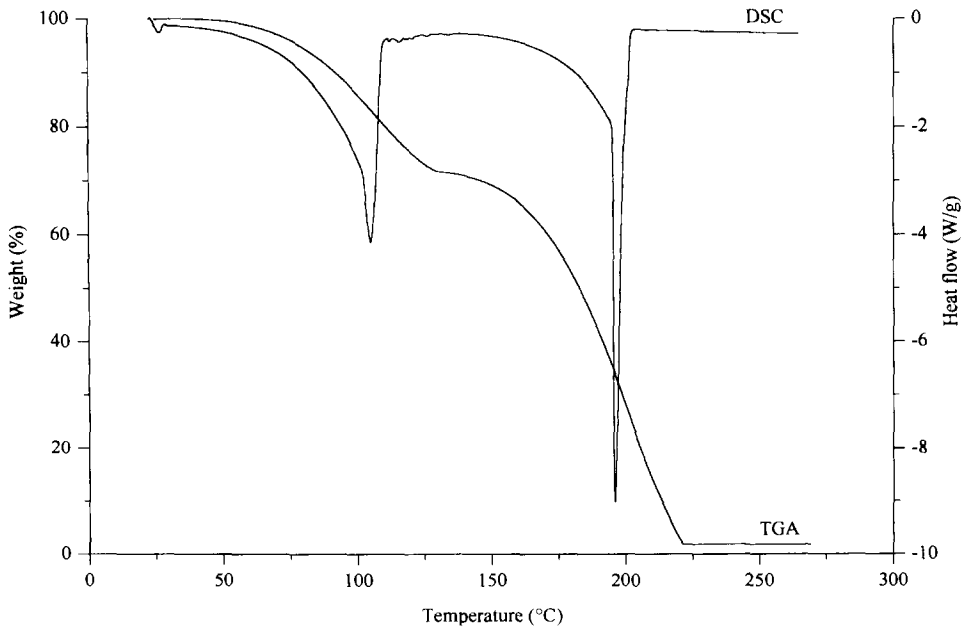

Fig. 8a. TGA–DSC of $H_2C_2O_4 \cdot 2H_2O$ in Ar; heating rate, 10°C min^{-1}.

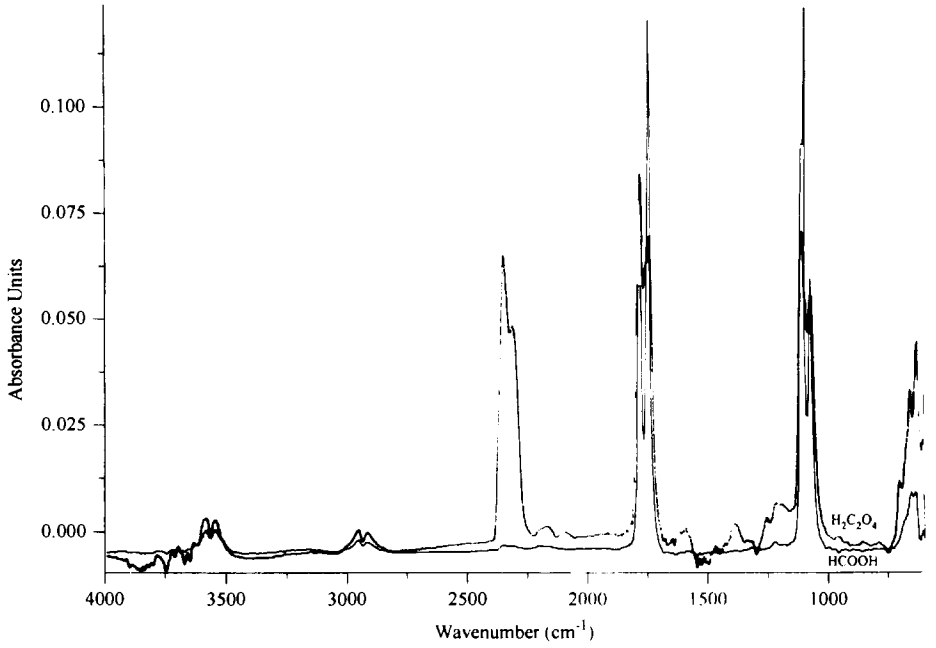

Fig. 8 b. FTIR spectrum of gases released by heating $H_2C_2O_4$ and by sublimation of HCOOH in Ar; heating rate, 10°C min^{-1}.

the low intensity) are found during the decomposition of the anhydrous acid salt, thereby confirming that reaction (5a) takes place. The FTIR spectrum of sample 6 also shows the release of CO ($\bar{\nu} = 2182$–$2114\ cm^{-1}$), which indicates that a second reaction takes place, namely the decomposition of oxalic acid with the release of H_2O, CO and CO_2, as represented in reaction (5b). As shown in Fig. 3 the second mass loss for $SrC_2O_4 \cdot yH_2C_2O_4 \cdot xH_2O$ (samples 4, 5, 6) at about 300°C increases with increasing value of y. At this temperature, H_2O, CO (both fragments of HCOOH) and CO_2 are released simultaneously, as indicated by the mass spectrum in Fig. 5.

For reaction (6a), the drop from the third to the fourth plateau (Fig. 3) corresponds to the evolution of both CO and CO_2, as shown by TGA–MS (Fig. 5) and TGA–FTIR (Fig. 6). As at this stage, because the temperature is still below the carbonate decomposition temperature, the detection of CO_2 must result from the CO disproportionation reaction (6b), which explains the exothermic signal in the DSC experiment (Fig. 7) between 500 and 550°C.

4.2.2. Decomposition of the carbonate

The last mass is attributed to the following reaction

$$SrC_2O_3 \xrightarrow[\text{endo}]{760\ 1058\ C} SrO + CO_2 \quad [\Delta m(7)\text{: theor. } 18.4\%\text{; exp. } 18.8\%] \qquad (7)^*$$

For reaction (7), in the TGA curve of sample 6 the high-temperature mass loss corresponds to 18.8% indicating that the final decomposition step is the formation of the oxide. By means of the FTIR spectrum corresponding to the conversion into the oxide (see Table 3), it is proven that only CO_2 is evolved. For the asymmetric stretching vibration of CO_2 [19], it is taken into account that the spectrum represents the P and Q bands and a good estimate of $\bar{\nu}_0$ is found at the minimum between two peaks. The bending vibration band has weak peaks on either side, which are difference bands involving the 667 cm^{-1} peak and two peaks at 1388 and 1285 cm^{-1} only active in the Raman spectrum [20]. The mass spectrometer monitors characteristic ion peaks at $m/e = 44$ and $m/e = 28$. The presence of the latter peak is consequently assigned to fragmentation of CO_2.

4.3. *Decomposition of the acid salt $SrC_2O_4 \cdot 1/2H_2C_2O_4 \cdot H_2O$ in O_2 (sample 6)*

The decomposition of the acid salt was also investigated in an oxidizing atmosphere. The FTIR spectrum showed the same peaks as for the decomposition under Ar. Heating sample 6 in O_2 at 10°C min^{-1} yields qualitatively the same results as shown in Fig. 5. The mass spectrum, however, showed that at the carbonate decomposition temperature, more CO_2 and less CO is detected in comparison with the decomposition in Ar. At this temperature, the FTIR spectrum showed a very strong peak at 2353 cm^{-1} due to CO_2 and two small peaks at 2178 and 2115 cm^{-1} resulting from CO. In the DSC experiment (Fig. 7), an exothermic signal is found between 400°C and 500°C. From these results, one can conclude that Eq. (6a) is immediately followed by the oxidation of CO to CO_2

$$CO + 1/2\ O_2 \underset{\text{endo}}{\overset{\text{exo}}{\rightleftharpoons}} CO_2 \qquad (8)^*$$

However, it is also possible that carbon produced from reaction (2a) is oxidized to CO_2

$$C + 1/2\ O_2 \underset{\text{endo}}{\overset{\text{exo}}{\rightleftharpoons}} CO_2 \qquad (9)^*$$

Acknowledgments

E. Knaepen is indebted to the "Vlaams Instituut voor de bevordering van het wetenschappelijk-technologisch onderzoek in de industrie (I.W.T)", Belgium for financial support. This text presents research results of the Belgian program on Interuniversity Poles of Attraction initiated by the Belgian State, Prime Minister's Office, Science Policy Programming. The scientific responsibility is assumed by its authors. This work is also supported by the Incentive Program on High Temperature Superconductors supported by the Belgian State Science Policy Office. The authors wish to thank Christel Willems and Hilde Pellaers respectively for the XRD and SEM measurements and Martine Vanhamel for her technical assistance.

References

[1] W.J. Schuele, J. Phys. Chem., 63 (1959) 83.
[2] J. Fransaer, J.R. Roos, L. Delaey, O. Van Der Biest, Arkens and J.P. Celis, J. Appl. Phys., 65 (1989) 3277.
[3] S. Hoste, H. Vlaeminck, P.H. De Ryck, F. Persyn, R. Mouton and G.P. Van Der Kelen, Supercond. Sci. Technol., 1(1989) 239.
[4] D.W. Johnson, Jr., and P.K. Gallagher, in Ceramic Processing Before Firing, John Wiley New York, 1978, p. 125–139.
[5] A. Vos, J. Mullens, J. Yperman, R. Carleer, J. Vanhees, L.C. Van Poucke, T.C. Krekels, G. Vantendoloo, F. Persijn, I. Van Driessche and S. Hoste, in B. Raveau *et al.*, (Eds.) Superconductivity, Technology Transfer Series, I.I.T.T.-T.C.M.A.S., Paris, 1991 p. 85.
[6] A. Vos, J. Mullens, R. Carleer, J. Yperman, J. Vanhees and L.C. Van Poucke, Bull. Soc. Chim. Belg., 101 (1992) 187.
[7] J. Mullens, A. Vos, A. De Backer, D. Franco, J. Yperman and L.C. Van Poucke, J. Therm. Anal., 40 (1993) 303.
[8] S.I. Hirano and T. Hayashi, Thermochim. Acta, 174 (1991) 169.
[9] L. Walter-Levy and J. Laniepce, C.R. Acad. Sci., 258 (1964) 217.
[10] J.C. Mutin and G. Watelle-Merion, C.R. Acad. Sci., Ser. C, 266 (1968) 315.
[11] A.S. Bhatti and D. Dollimore, Thermochim. Acta, 78 (1984) 63.
[12] A. Vos, J. Mullens, R. Carleer, J. Yperman, J. Vanhees and L.C. Van Poucke, Bull. Soc. Chim. Belg., 101 (1992) 3.
[13] De Wolff, Technische Physische Dienst, Netherlands, JCPDS Grand-in-Aid-Report.
[14] L. Walter-Levy and J. Laniepce, C.R. Acad. Sci., 257 (1963) 910.
[15] J. Mullens, A. Vos, R. Carleer, J. Yperman and L.C. Van Poucke, Thermochim. Acta, 207 (1992) 337.
[16] D. Dollimore, G.R. Heal and N.P. Passalis, Thermochim. Acta, 92 (1985) 543.
[17] D. Dollimore and D.L. Griffiths, J. Therm. Anal., 2 (1970) 229.
[18] E. Knaepen, J. Mullens, J. Yperman and L.C. Van Poucke, Proceedings NATAS, San Francisco, (1995), p. 394.
[19] K. Nakamoto, Infrared Spectra of Inorganic and Coordination Compounds, Wiley Interscience, 1970, p. 78, 83 and 89.
[20] N.B. Colthup, L.H. Daly and S.E. Wiberley, Introduction to Infrared and Raman Spectroscopy, Academic Press, San Diego, p. 31 and 310.